Hindawi
Journal of Nanomaterials
Volume 2019, Article ID 4546350, 14 pages
https://doi.org/10.1155/2019/4546350

Research Article

A Theoretical Study on the Inclusion of Fe, Cu, and Zn in Illite Clays

Antonio Sánchez-Coronilla,[1] **Elisa I. Martín**,[2] **Francisco José Fernández-de-Cordova**,[3] **Francisco Javier Santos**,[1] **and José Hidalgo Toledo**[1]

[1]*Departamento de Química Física, Facultad de Farmacia, Universidad de Sevilla, E-41012 Sevilla, Spain*
[2]*Departamento de Ingeniería Química, Facultad de Química, Universidad de Sevilla, E-41012 Sevilla, Spain*
[3]*Instituto de Investigaciones Químicas (IIQ), CSIC-Universidad de Sevilla, Avenida Américo Vespucio 49, E-41092 Sevilla, Spain*

Correspondence should be addressed to Antonio Sánchez-Coronilla; antsancor@us.es and Elisa I. Martín; elisamf@us.es

Received 14 December 2018; Accepted 28 March 2019; Published 7 May 2019

Academic Editor: Ruibing Wang

The inclusion of Fe, Cu, and Zn in (1, 0, 0), (0, 0.5, 0), and (0.5, 0.5, 0.5) sites of an illite with the $KAl_2Si_4O_{12}H_2$ structure has been studied. For the inclusion of the metals, their common oxidation states were chosen, that is, 0, +2, +3 and 0, +1, +2, for Fe and Cu, respectively, while 0 and +2 for Zn. Periodic DFT calculations were performed to know the most favourable site of incorporation of the ions. Energetically the most favourable site for the inclusion corresponds to the (1, 0, 0) coordinate for all the ions independently of their oxidation state. However, the highest oxidation state of the metals (Fe^{3+}, Cu^{2+}, and Zn^{2+}) was the most favoured for being incorporated into the illite structure and was the selected ion for the discussion. In those structures, metal oxygen interaction plays an important role in stabilizing the systems. Structural and energetic results indicate that illite presents good adsorption characteristic of those Fe^{3+}, Cu^{2+}, and Zn^{2+} in the (1, 0, 0) site. Thus, those ions may be available for plants for its extraction by phytoextraction techniques and the consequent soil regeneration. The inclusion of a second metallic ion revealed the most favourable inclusion corresponding to the inclusion of Fe^{3+} ion. The inclusion of this ion modifies the coordination sphere around the first metal being available for subsequent extraction by phytoremediation or other techniques for clean-up of the soil and its regeneration.

1. Introduction

Clay minerals are major components in soils and sedimentary rocks [1]. They play an important role in environmental processes such as nutrient cycling, plant growth, organic matter maturation, contaminant migration, and petroleum production and could coexist with methanogens in anoxic environments [2, 3]. Of relevance is the role played in methane adsorption and radionuclide adsorption on clay rocks [4, 5]. The latter is related to their use as sealing barriers in nuclear waste and spent nuclear fuel repositories [5]. Regarding the protective effect of mineral clays, illite is one of the clays that best counteract the disruption of the intestinal barrier permeability caused by mycotoxins [6].

Illite is a common soil component [1]. Illite is a natural and available mineral in the world with a variety of physicochemical characteristics such as porosity, small particle size, good bonding ability, great electrical insulating property, and thermal stability [7]. Illite is found as abundant phase in natural clays as a consequence of the transformation of smectite with general formula $K_yAl_4(Si_{8-y},Al_y)O_{20}(OH)_4$ usually with $1 < y < 1.5$, but always with $y < 2$ where potassium is commonly localized in interlayer sites [8]. Silicon is replaced by aluminum isomorphically in the tetrahedral layer to maintain global charge [9]. It is of note that soils where illite is the predominant phase are characterized by high adsorption and low desorption capacities [10]. This clay has been used as a low-cost adsorbent for industrial waste treatment and as adsorbent for fast and efficient removal of phosphate from aqueous solution [10]. The phosphate adsorption is pH-dependent, and illite shows a great potential as adsorbent [11].

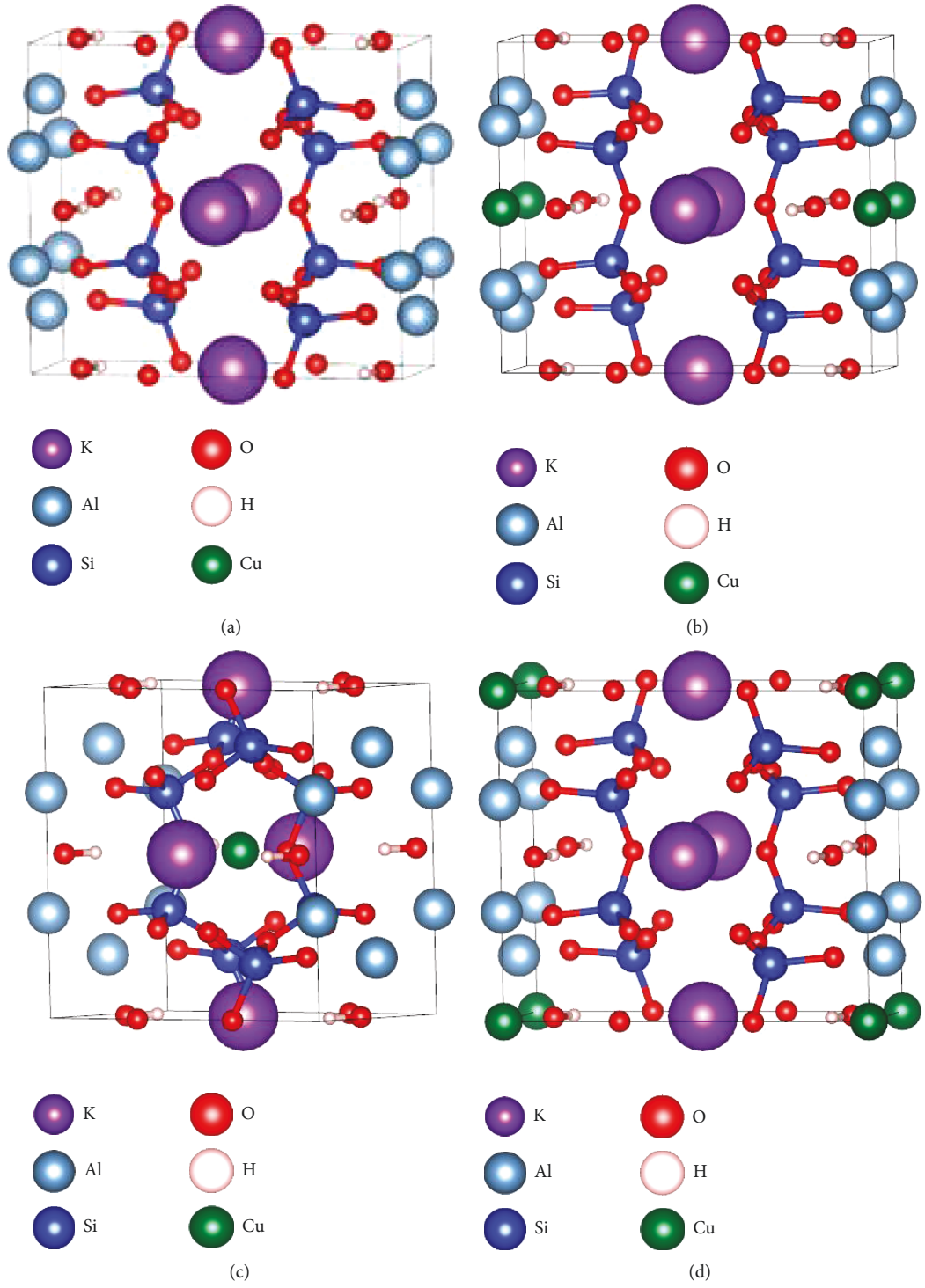

FIGURE 1: The local geometry for illite, $KAl_2Si_4O_{12}H_2$ (a). Coordinates for the inclusion of Cu into the illite structure: (b) (0, 0.5, 0), (c) (0.5, 0.5, 0.5), and (d) (1, 0, 0).

Soil contamination by heavy metals (As, Cd, Cr, Cu, Pb, and Zn) is one of the major environmental problems raising critical concerns for both human health and ecosystems due to their carcinogenic and mutagenic effects on animals and humans. The clean-up of most of these soils is mandatory for the area to be reclaimed and to minimize the entry of potentially toxic elements into the food chain [12–15]. Thus, polluted soils by metals are a source of negative environmental impact. These metals can pollute groundwater and aquifers with consequent environmental disaster. Therefore, both the extraction of heavy metals from polluted soils and a consequent regeneration of the contaminated soils have attracted the interest of researchers for the last years [16–18]. In fact, a greenhouse technique for recovering

polluted soils based on the use of plant is phytoremedation [12, 18]. Phytoremediation is both an efficient and an economically feasible method that can be used for the removal of heavy metals and radionuclides as well as for organic pollutants such as polynuclear aromatic hydrocarbons, polychlorinated biphenyls, and pesticides [12, 18, 19]. Terrestrial plants have the capacity of adsorbing heavy metals present in the soil [14, 20]. This capacity depends on chemical factors such as the nature of the different metals and their availability within the structure of the soils. Therefore, the sorption/desorption of the metals depends on their nature, that is, the oxidation state of those metals [13, 14, 17, 21].

Thus, the earlier review of literature reveals the key role that plays the sorption and fixation of the metals into the soils for being extracted and the next soil regeneration. In this sense, it is of interest to know both how the metals are distributed into the clay and their oxidation state.

In this study, an illite clay with composition $KAl_2Si_4O_{12}H_2$ has been selected. Periodic calculations based on the density functional theory (DFT-periodic) were performed to know how the presence of some metals affects the illite structure. The chosen metals were Fe, Cu, and Zn due to their usual presence in soils near mining wastes. We have studied the inclusions of these metals individually and their combination in pairs. The individual atoms have been examined with different oxidation states and placed in the initial structure in different positions. Both the energetically more stable oxidation state and the metal position inside illite were selected. The positions of the individual atoms served as the initial point for the combination of the two metals. Finally, the electronic effect of the metals into the illite structure was explored through the electron localization function (ELF) and density of states (DOS) analysis.

2. Materials and Methods

2.1. Computational Framework. DFT-periodic calculations were performed using the Vienna Ab Initio Simulation Package (VASP) with the projector-augmented wave (PAW) method [22, 23]. The number of plane waves in VASP was controlled by a cut-off energy, set in our calculations to E_{cut} = 500 eV to satisfactorily describe the system. The electron exchange and correlation were treated within the generalized gradient approximation (GGA). In the case of GGA, Perdew-Burke-Ernzerhof (PBE) functional was used. Both the cell shape and atomic positions were optimized using a conjugate-gradient algorithm, where the iterative relaxation of atomic positions was stopped when the forces on the atoms were less than 0.01 eV/Å. Gaussian smearing with $k_BT = 0.1$ eV was applied [22–25].

Illite ($KAl_2Si_4O_{12}H_2$) was characterized by the C2/m space group [26]. The tag KSPACING determined the number of k-points in the mesh. A value of 0.3 for sampling the Brillouin zone for the illite bulk was enough to obtain negligible changes in the optimized cell parameters and energy. The resulting cell parameters were $a = 5.312$ Å, $b = 8.868$ Å, and $c = 10.401$ Å with $\alpha = \gamma = 90^\circ$; $\beta = 100.55^\circ$, in agreement with the experimental values ($a = 5.202$ Å, $b = 8.979$ Å, $c = 10.226$ Å; $\alpha = \gamma = 90^\circ$; $\beta = 101.57^\circ$) [26]. The metals Fe, Cu, and Zn were chosen, and the effect of its inclusion in the illite structure was studied from three positions that correspond to the coordinates (0, 0.5, 0), (0.5, 0.5, 0.5), and (1, 0, 0) in the unit cell. The density of states (DOS) and projected density of states (PDOS) for the relaxed structures were obtained using the tetrahedron method with Blöchl corrections and a KSPACING of 0.2. Electron localization function (ELF) images and structure images were obtained using the Vaspview software and Vesta, respectively [27, 28].

Table 1: Difference in energy for the inclusion of the metals in different sites of the illite structure.

	ΔE (eV)		
	(0, 0.5, 0)	(0.5, 0.5, 0.5)	(1, 0, 0)
Fe^{3+}	-28.35	-28.84	-31.59
Fe^{2+}	-22.62	-24.46	-28.08
Fe^0	-11.80	-15.97	-16.02
Cu^{2+}	-17.13	-20.71	-22.40
Cu^+	-16.79	-20.05	-21.13
Cu^0	-7.03	-10.97	-12.54
Zn^{2+}	-19.91	-20.39	-23.84
Zn^0	-4.49	-10.87	-10.90

3. Results and Discussion

3.1. Inclusion of Fe, Cu, and Zn in the Illite Structure. The inclusion of Fe, Cu, and Zn in the illite structure has been performed in three different coordinates, which are (0, 0.5, 0), (0.5, 0.5, 0.5), and (1, 0, 0) in the illite cell. Figure 1 shows the local geometry for the most stable configuration of the optimized illite structure. Also in this figure, the local geometry inclusion of Cu is shown as an example of the positions of the metals within the cell.

The common oxidation states of Fe, Cu, and Zn were selected for their inclusion into the illite structure. Thus, for the inclusion of Fe and Cu, three oxidation states were chosen: 0, +2, +3 and 0, +1, +2, respectively, with only two states for Zn, that is, 0 and +2. To gain insight into the energetics of the effect of the inclusion of the metals in the illite structure, the difference in energy as consequence of the inclusion of the metals in the three coordinates was calculated as follows:

$$\Delta E = E_{(\text{metal/illite})} - E_{(\text{illite})}, \quad (1)$$

where $E_{(\text{metal/illite})}$ and $E_{(\text{illite})}$ are the total energies of the illite structure with the metal and free, respectively. The differences in energy for the different metals are included in Table 1.

According to the energetic results shown in Table 1, the most favoured site for the adsorption of the metals corresponds to the coordinate (1, 0, 0). In the case of Zn^0, similar results were obtained for the inclusion in coordinates (0.5, 0.5, 0.5) and (1, 0, 0), with the inclusion in the latter coordinate being slightly more stable. Of note is that in all positions,

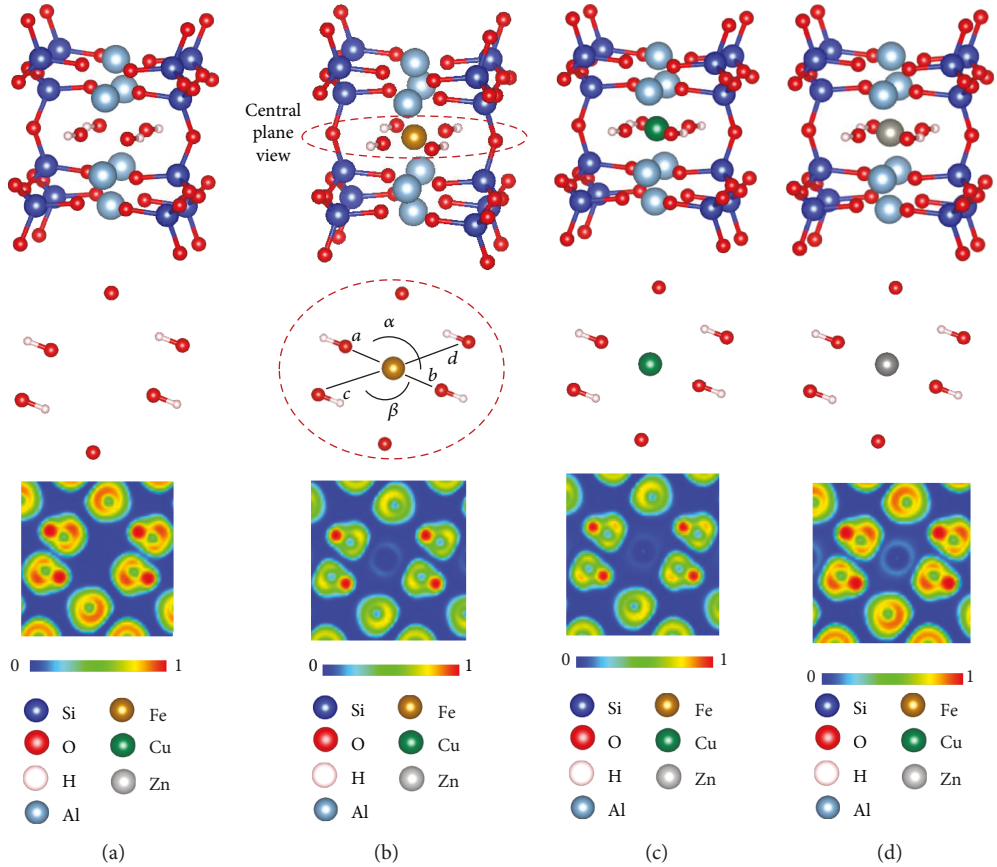

Figure 2: The local geometry around the (1, 0, 0) inclusion site with the ELF contour plots from the central plane view of (a) illite, (b) Fe^{3+}, (c) Cu^{2+}, and (d) Zn^{2+}.

Table 2: Geometrical parameters, identified in Figure 2, of the structures studied.

Structure	Distance (Å)				Angle (°)	
	a	b	c	d	α	β
Fe^{3+}	2.27301	2.27290	3.43240	3.43234	179.9952	179.9964
Cu^{2+}	2.27344	2.27328	3.43260	3.43154	179.9071	179.9410
Zn^{2+}	2.27353	2.27332	3.43314	3.43300	179.9970	179.9966

the highest oxidation state of the metals (Fe^{3+}, Cu^{2+}, and Zn^{2+}) is the most favoured for being incorporated into the illite structure. This result is of interest because it implies a major availability of those elements in the illite structure for being extracted, which agrees with experimental results of desorption of those metals [5, 14, 19, 21, 29]. In this way, from now on the discussion of the results will be mainly focused on the inclusion of the highest oxidation states of the metals. Figure 2 shows the local geometry in the coordination shell around Fe^{3+}, Cu^{2+}, and Zn^{2+} for the most stable configuration of the optimized structures in the coordinate (1, 0, 0) of the illite structure. For the purpose of comparison, the figure also includes the illite structure. As an example, the HO-M-OH angles and M-OH distances (M = Fe^{3+}, Cu^{2+}, and Zn^{2+}) of the cut corresponding with the middle face of the structures as indicated in the dotted circle in Figure 2 are shown in Table 2. As Table 2 shows, α and β angles hardly change and are around 180°. In addition, it is also observed that, generally, the M-OH distances are slightly shorter for the inclusion of Fe^{3+} than for Cu^{2+} and Zn^{2+}. Moreover, the (001) basal distance for the systems after the incorporation of Fe^{3+}, Cu^{2+}, and Zn^{2+} ions is 10.10053, 10.15051, and 10.15604 Å, respectively. Such results suggest a strengthening of the interactions between the metals and the oxygen, which may be thought to be exclusively due to the smaller ionic radii of Fe^{3+} than Cu^{2+} and Zn^{2+}, but it is also necessary to consider electronic effects produced in the structures, as will be discussed below from the ELF and PDOS. Thus, the ELF plot in 2D corresponding to the M-OH (M = Fe^{3+}, Cu^{2+}, and Zn^{2+}) interactions for the inclusion in the (1, 0, 0) site of illite is shown in Figure 2. In this figure, the contour plot around the oxygen atoms is different for the systems with Fe^{3+}, Cu^{2+}, and Zn^{2+} when it is compared with those of illite. There is a modification of the halos of the contour plot

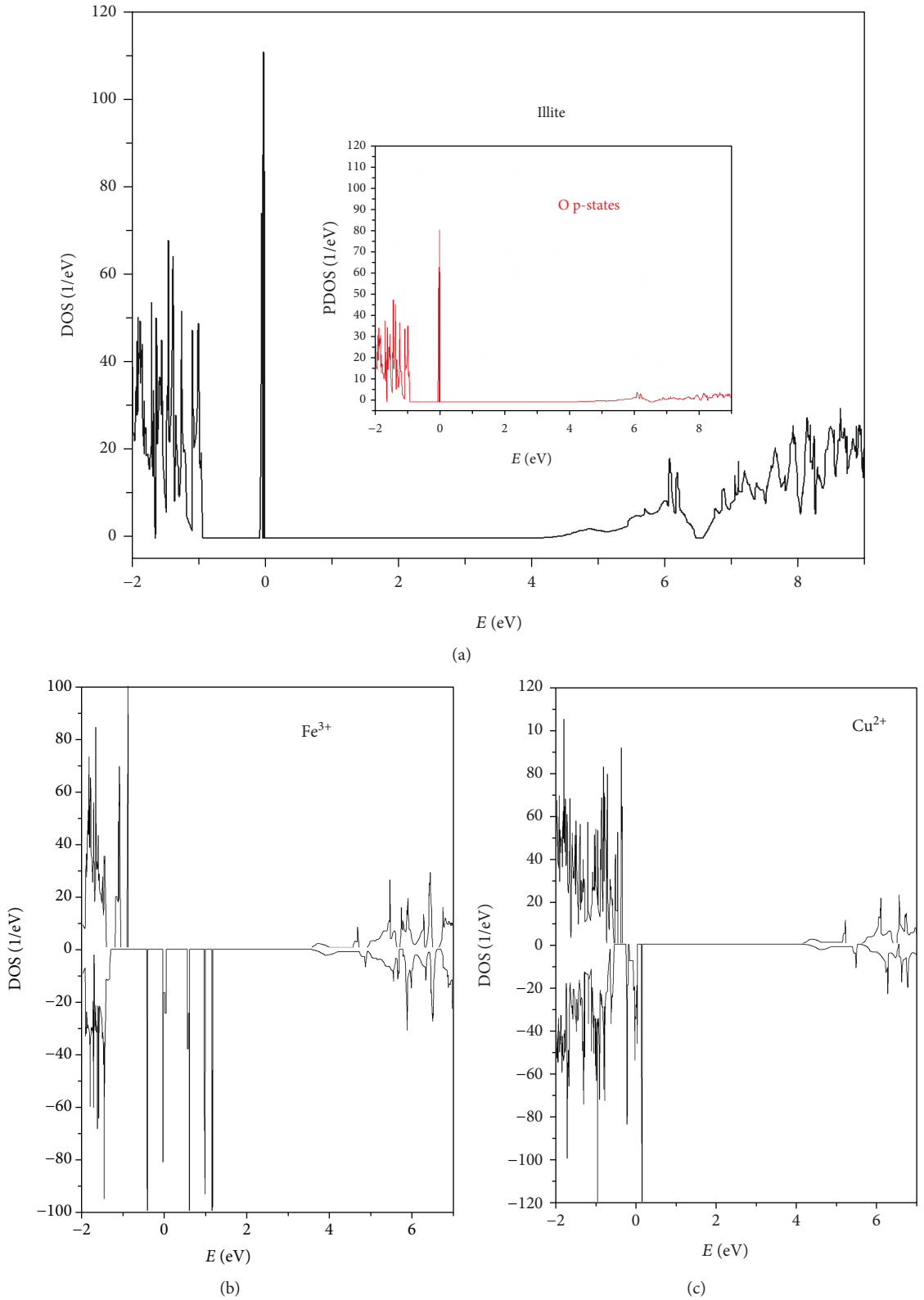

Figure 3: Continued.

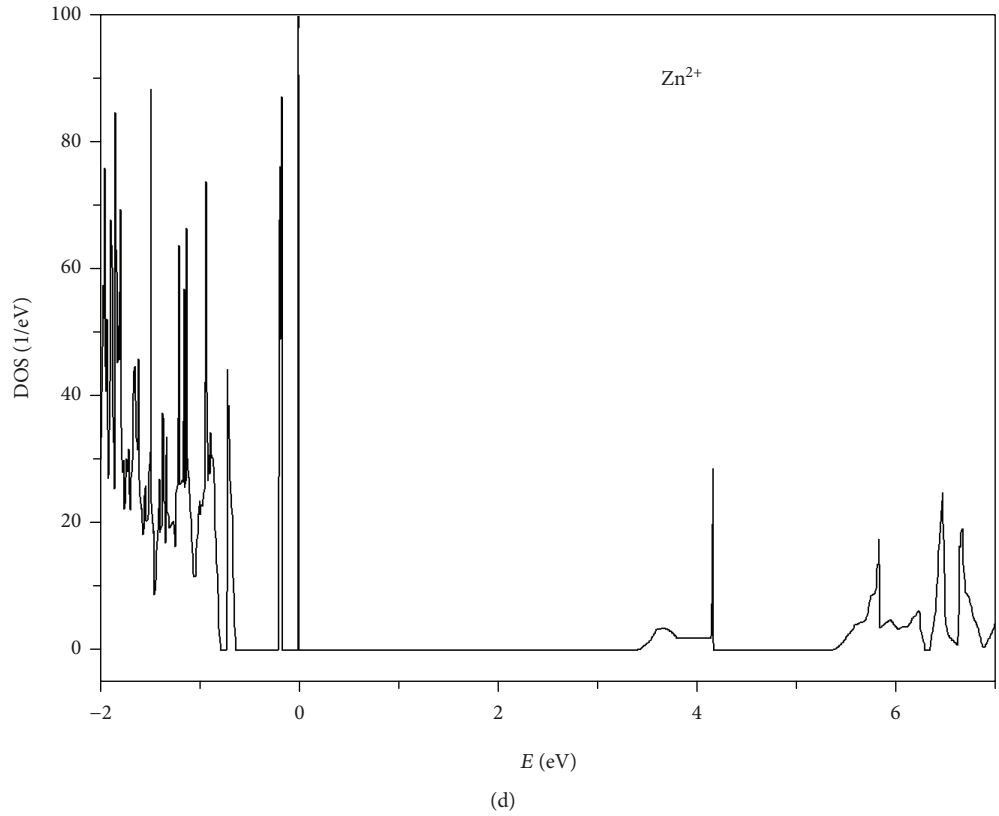

(d)

Figure 3: Total DOS plot for (a) illite and the inclusion of (b) Fe^{3+}, (c) Cu^{2+}, and (d) Zn^{2+} in the (1, 0, 0) site. In the inset: PDOS of the O p-states from illite.

towards Fe^{3+} and Cu^{2+} by means of slight electron localization (sky blue colour) which provides stability to the metal-oxygen interaction. This highlights an attraction between the oxygen and the metals which explains the geometrical results expounded above (Table 2). The contour plot ELF for the system with Zn^{2+} resembles that of illite. However, there is also a slight directionality in the outlines of the electron localization of oxygen towards Zn^{2+}. ELF analysis indicates the strengthening of the interaction between the oxygen atoms from illite and metals. The inclusion of the metals in other coordinates causes distortion of the structure as compared to the parent structure. As an example, the structural distortion is clearly reflected in the variation in the Fe-OH distances (ca. 1.66 and 1.67 Å, for *a* and *b* in Figure 2, respectively) and HO-Fe-OH angles (ca. 172.33°) of the central plane view for the inclusion of Fe^{3+} in the (0, 0.5, 0) site. That distortion of the structure is related to structural tensions and thereby with instability. Thus, it is understandable that the inclusion of the metals in the (1, 0, 0) site leads to the most stable structures with the minimal geometrical differences when compared to the illite structure.

To further understand the electronic properties that underlie the metal-oxygen interactions, the electronic structure of the inclusion of Fe^{3+}, Cu^{2+}, and Zn^{2+} in the (1, 0, 0) site will be discussed by means of DOS and PDOS (Figure 3). The illite band gap is around 4.2 eV (Figure 3(a)). The analysis of the projected density of states (PDOS) on the oxygen atoms of illite indicates that the valence and conduction bands are mostly composed of the O p-states (inset of Figure 3(a)). With the inclusion of the metals appear new bands in the gap for the inclusion of Fe^{3+} and Cu^{2+}, while for the inclusion of Zn^{2+} only a new band near the valence band maximum appears (Figure 3). The presence of bands in the gaps for the inclusion of Fe^{3+} led to the existence of new lower-energy electronic transition with the lowest band gap value around 2.3 eV, followed by the systems with Zn^{2+} and Cu^{2+}, ca. 3.5 and 3.9 eV, respectively (Figure 3). This energy electronic transition should lead to changes in the experimental UV-Vis absorption spectra as compared to that of illite. In this sense, experimental band gap values can be obtained both by using UV-Vis spectra in reflectance diffuse mode, determined as reported elsewhere [30], and finally by comparing with those obtained in the calculations. The distribution and the chemical interaction of the metals within the structure are of interest because a rich transfer of the metals during water movement along the soil pore may exist, which has been previously shown by optical measurements in surface and subsurface soil horizons [31]. The analysis of PDOS for the inclusion of Fe^{3+} and Cu^{2+} reveals that those bands in the gap belong mostly to the contribution of Fe^{3+} and Cu^{2+} d-states that overlap with the bands from the O p-states (Figures 4(a) and 4(b)). This overlapping is indicative of the oxygen metal interaction which agrees with the above discussion from ELF analysis. A different situation is obtained from the analysis of the PDOS for the inclusion of Zn^{2+} (Figure 4(c)). The presence of Zn^{2+} in the illite structure

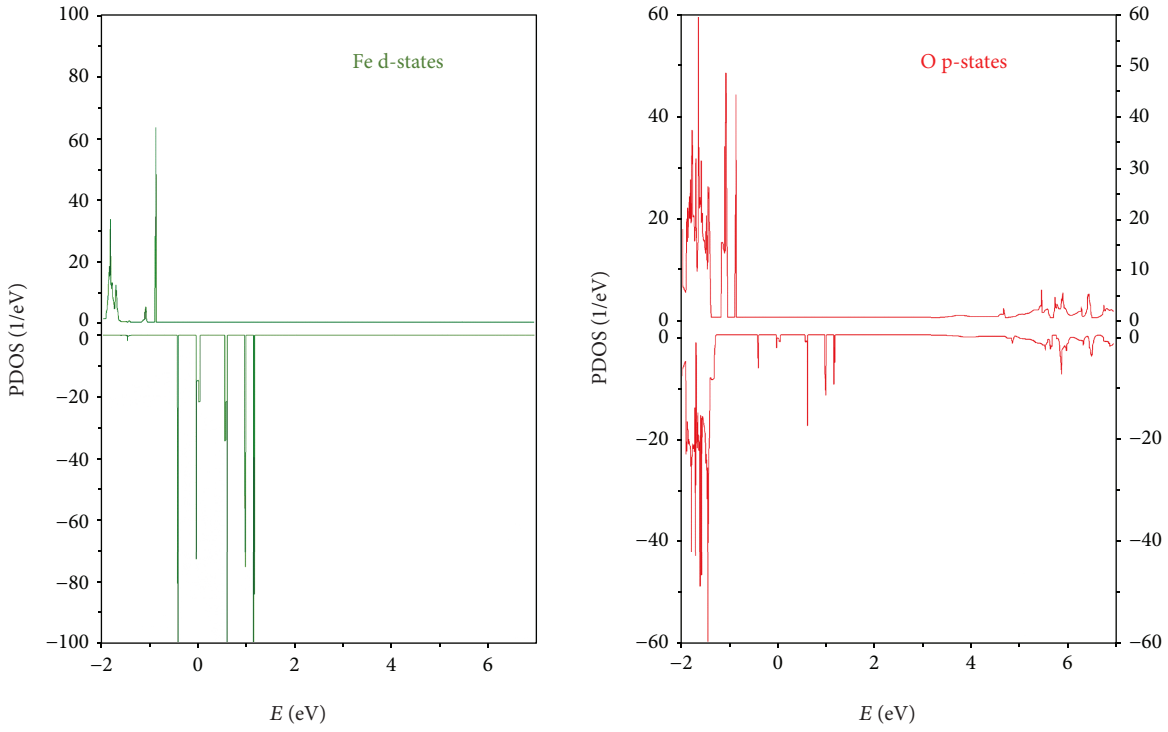

(a)

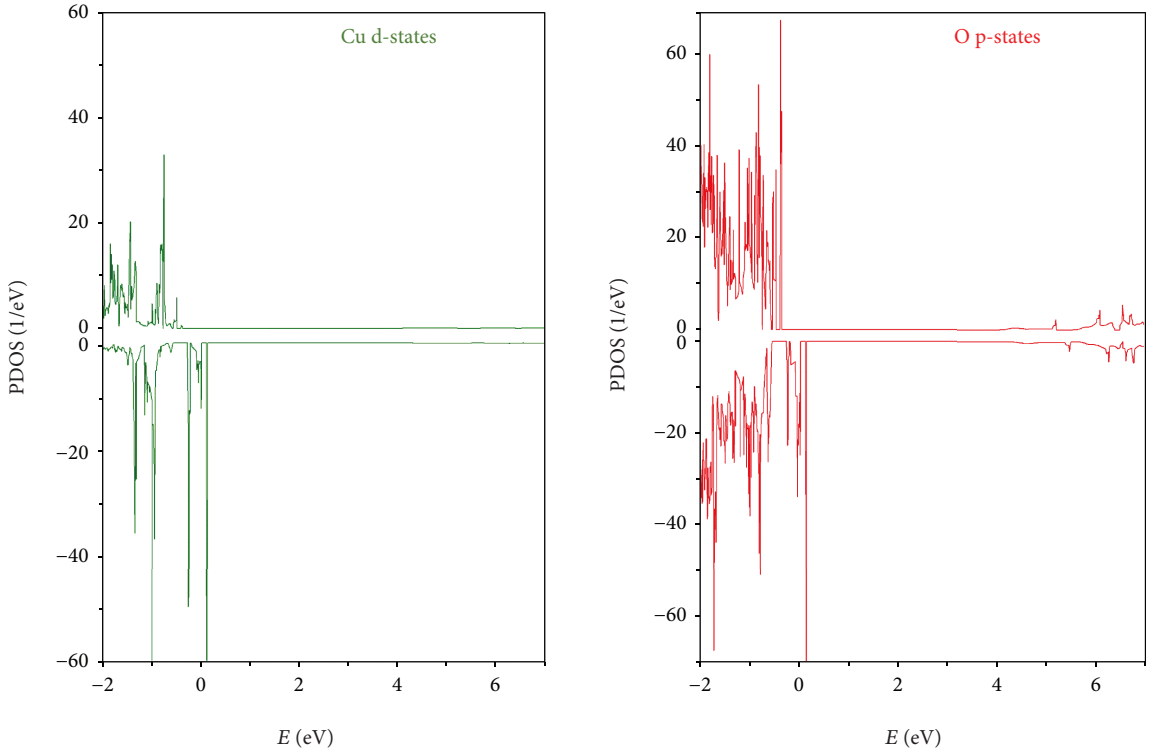

(b)

Figure 4: Continued.

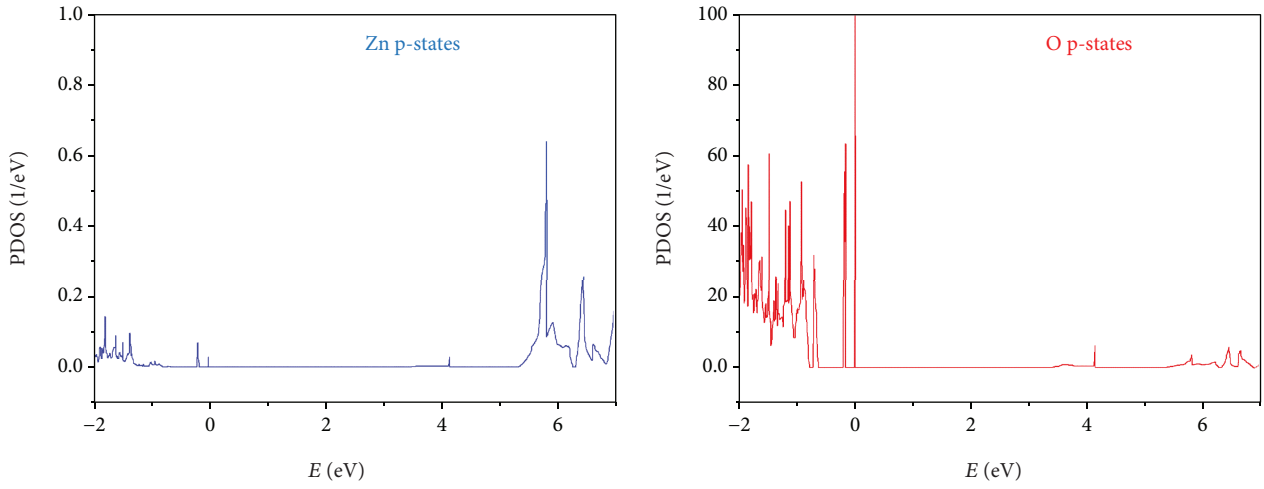

(c)

Figure 4: PDOS plot for the inclusion of (a) Fe^{3+} (b) Cu^{2+}, and (c) Zn^{2+} in the (1, 0, 0) site.

indicates the main contribution of the Zn p-states to the edge of the valence band that overlap with the bands from the O p-states of the structure (Figure 4(c)), revealing the interaction between the Zn and oxygen atoms in the structure, as stated above.

Finally, based on this structural and energetic discussion, it seems reasonable to consider that illite presents a good adsorption character of those metals (Fe^{3+}, Cu^{2+}, and Zn^{2+}) in the (1, 0, 0) site. Therefore, for instance, those metals may be available for plants for its extraction by using phytoextraction techniques and the consequent soil regeneration.

3.2. Inclusion of a Second Fe, Cu, and Zn Atom in the Illite Structure. As far as metallic compounds are hard to be found alone, it is of interest to explore the effect that the presence of two metallic atoms has on the illite structure. From the results expounded above, the structures with Fe^{3+}, Cu^{2+}, and Zn^{2+} in the (1, 0, 0) site for exploring theoretically the changes in the structural and electronic properties of the illite when a second metallic (Fe, Cu, or Zn) atom is included were selected. The oxidation state selected for the inclusion of the second element was Fe^{3+}, Cu^{2+}, and Zn^{2+} based on the energetic analysis shown above. In order to evaluate the structural changes ought to the presence of two metals, site (0, 0.5, 0) was selected for the inclusion of the second metal. For the study, we selected the (0, 0.5, 0) site instead of the (0.5, 0.5, 0.5) site because the potassium atoms in the latter will be placed around the metals and they may hinder the electronic interactions between the two metals.

The local geometry for the most stable configuration of the optimized structures for the incorporation of the second Fe^{3+}, Cu^{2+}, and Zn^{2+} ions is shown in Figure 5. In Table 3 is included the difference in energy when a second metal is included in the illite structure. This difference is defined as

$$\Delta E = E_{(\text{metal/metal/illite})} - E_{(\text{metal/illite})}, \quad (2)$$

where $E_{(\text{metal/metal/illite})}$ and $E_{(\text{metal/illite})}$ are the total energies of the illite structure with the two metals and with only one, respectively. According to the results shown in Table 3, the most stable interactions correspond to those systems with the inclusion of the second Fe^{3+} ion (structures **1**, **5**, and **8** in Figure 5). The inclusion of the second atom modifies slightly the illite structure. The most striking changes are produced around the metals, so attention will be drawn to the Al atoms around the metals, as indicated in the central plane view of Figure 6. The geometrical changes for structures **1**, **5**, and **8** are shown in Table 4. The inclusion of the second Fe^{3+} decreases the Al-Fe distances (*a* and *b* in Figure 6) in the following order **1** > **8** > **5**, with angle α from Figure 6 next to 180° for structure **5**, with this structure being the most favoured energetically, in agreement with the energetic data from Table 3. The shortening of distances *a* and *b* in Figure 6 is accompanied by an increase in the values in the distances between Al-M (M = Fe, Cu, and Zn), namely, *c* and *d* in Figure 6. Although the second Fe^{3+} ion is surrounded by Al cations, Fe^{3+} is stabilized by the two hydroxyl groups placed around this ion, as the distances around 1.7-1.8 Å for all systems are attested (e and f in Table 4), and this will be corroborated below by the PDOS analysis. The ELF analysis reveals the existence of electron localization (green and sky blue colour) between the Al and Fe atoms in structures **1**, **5**, and **8** (dotted square in Figure 6). This result implies a certain degree of stabilizing interactions in the system by a redistribution of electronic localization focusing from Al towards Fe which enables its interaction with the two hydroxyl groups from structures **1**, **5**, and **8**. Thus, the inclusion of the second metal performs a kind of synergistic effect in the illite structure with regards the accommodation of the other metals in the structure for being available for a subsequent extraction by phytoremediation or other techniques.

Finally, the possible electron changes originated by the presence of a second metal in the illite structure were analysed by means of DOS (Figure 7). The incorporation of Fe^{3+} modifies the gap of illite with the appearance of new bands near the edge of the valence band for the three structures (**1**, **5**, and **8**). Those bands are mainly from the Fe and

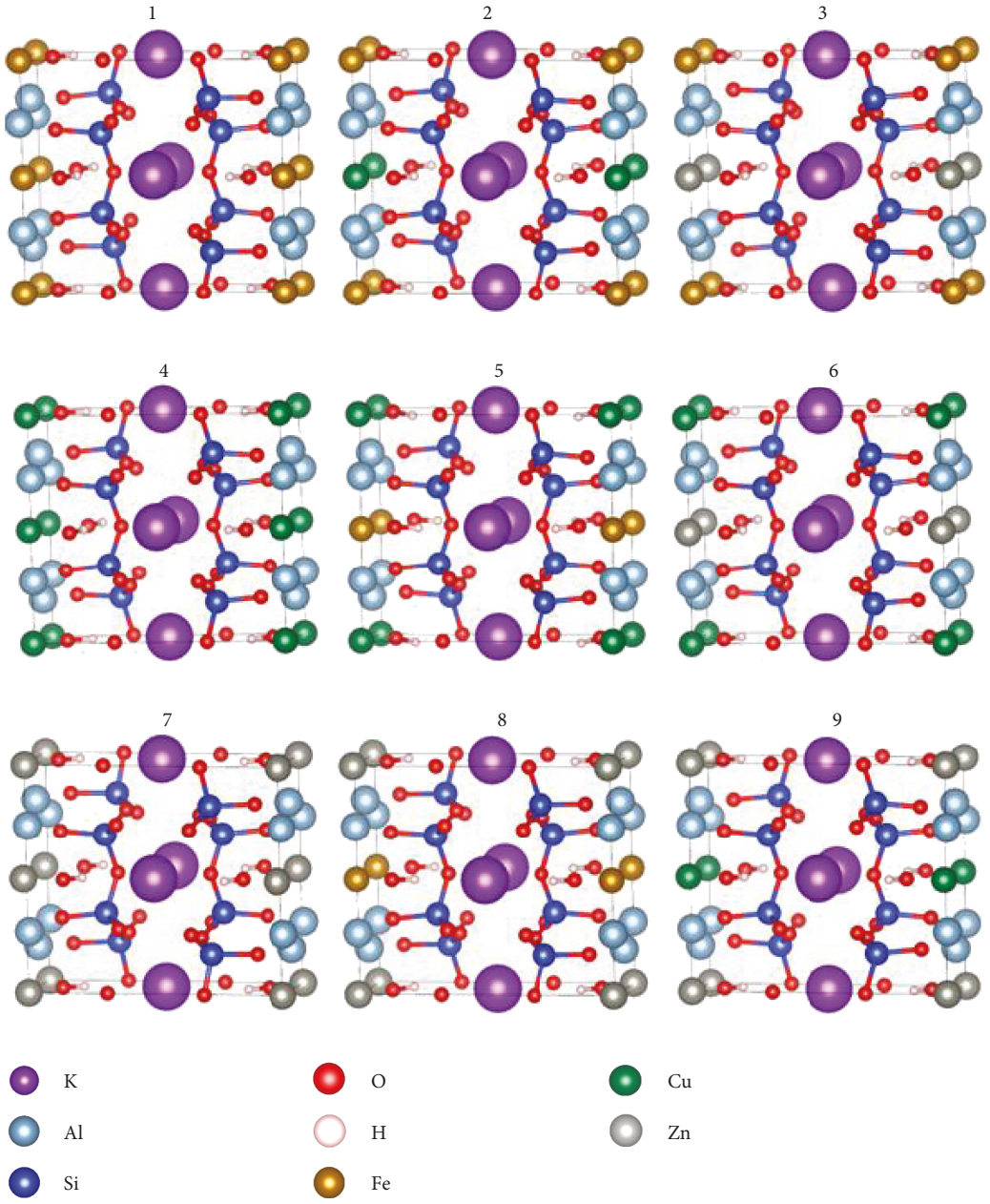

Figure 5: The local geometry for the second inclusion of Fe^{3+}, Cu^{2+}, and Zn^{2+} ions in the (0, 0.5, 0) site for the structures with Fe^{3+} (from 1 to 3), Cu^{2+} (from 4 to 6), and Zn^{2+} (from 7 to 9) in the (1, 0, 0) site.

Table 3: Difference in energy when a second metal is included in the illite structure as shown in Figure 5.

Structure	ΔE (eV)
1	-10.78
2	-3.46
3	-2.20
4	-6.80
5	-13.49
6	-1.73
7	-3.71
8	-12.23
9	-1.72

O d- and p-states, respectively (Figure 8). The overlaps of those bands corroborate with the Fe-O interaction for the inclusion of the second metal and the stabilization of the system.

4. Conclusions

This paper presents the theoretical study of the stability and electronic effect of the inclusion of Fe, Cu, and Zn in different sites of an illite with the $KAl_2Si_4O_{12}H_2$ structure. Three sites were selected in the illite structure, namely, (1, 0, 0), (0.5, 0.5, 0.5), and (0, 0.5, 0). For the inclusion of the metals, their common oxidation states were chosen: 0, +2, +3 and 0, +1, +2, for Fe and Cu, respectively, while for Zn, only two states

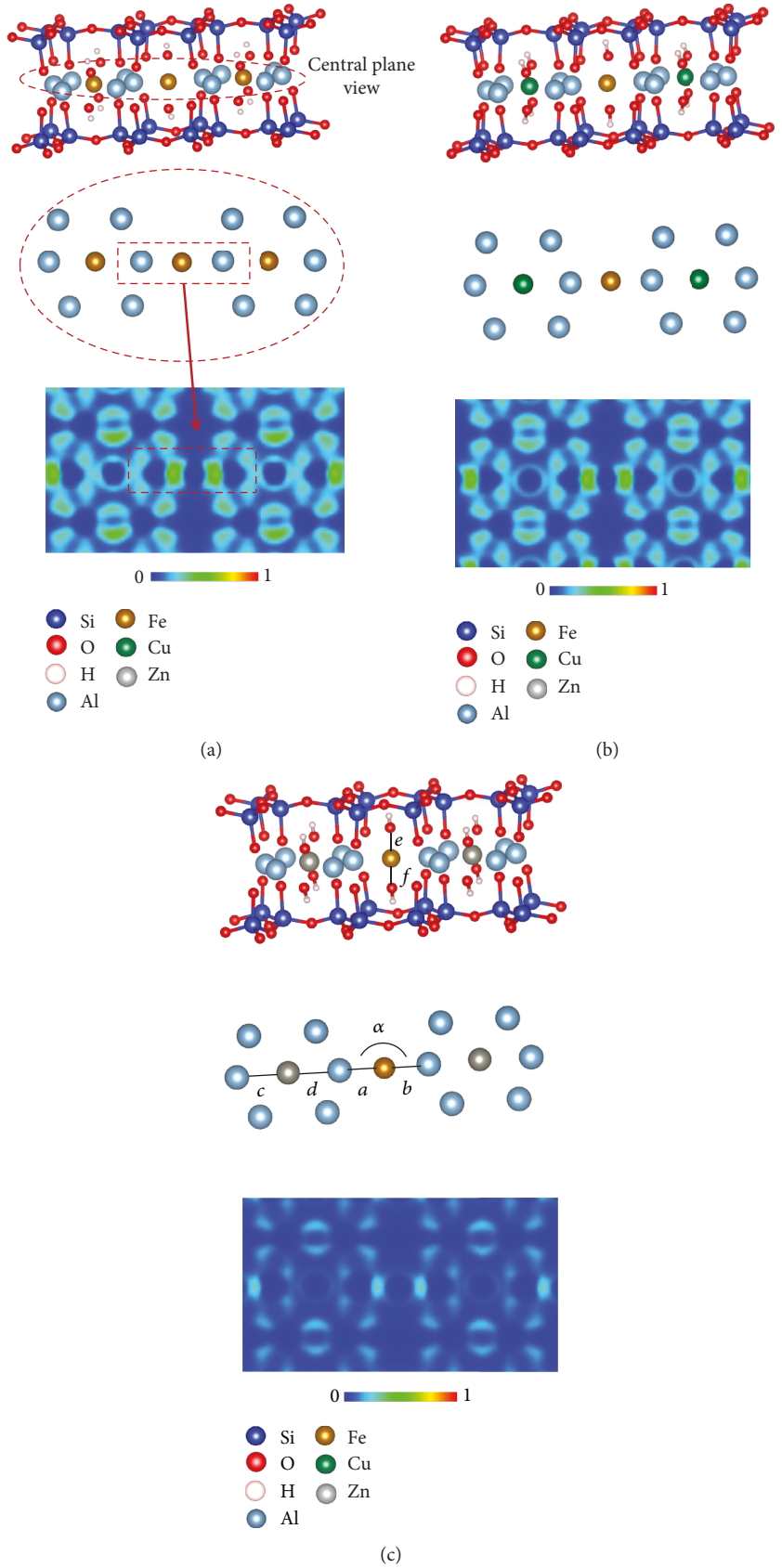

FIGURE 6: The local geometry around the (0, 0.5, 0) inclusion site with the ELF contour plots from the central plane view of structures **1** (a), **5** (b), and **8** (c) from Figure 5.

Table 4: Geometrical parameters, identified in Figure 6, of structures **1**, **5**, and **8**. Distances *e* and *f* are indicated inside Figure 6(c).

Structure	Distance (Å)						Angle (°)
	a	*b*	*c*	*d*	*e*	*f*	*α*
1	2.08214	2.06512	2.34901	2.37683	1.73931	1.72281	175.0576
5	2.02611	2.05500	2.38037	2.41132	1.69137	1.70156	178.9922
8	2.06015	2.06605	2.37360	2.37155	1.75176	1.79985	176.2542

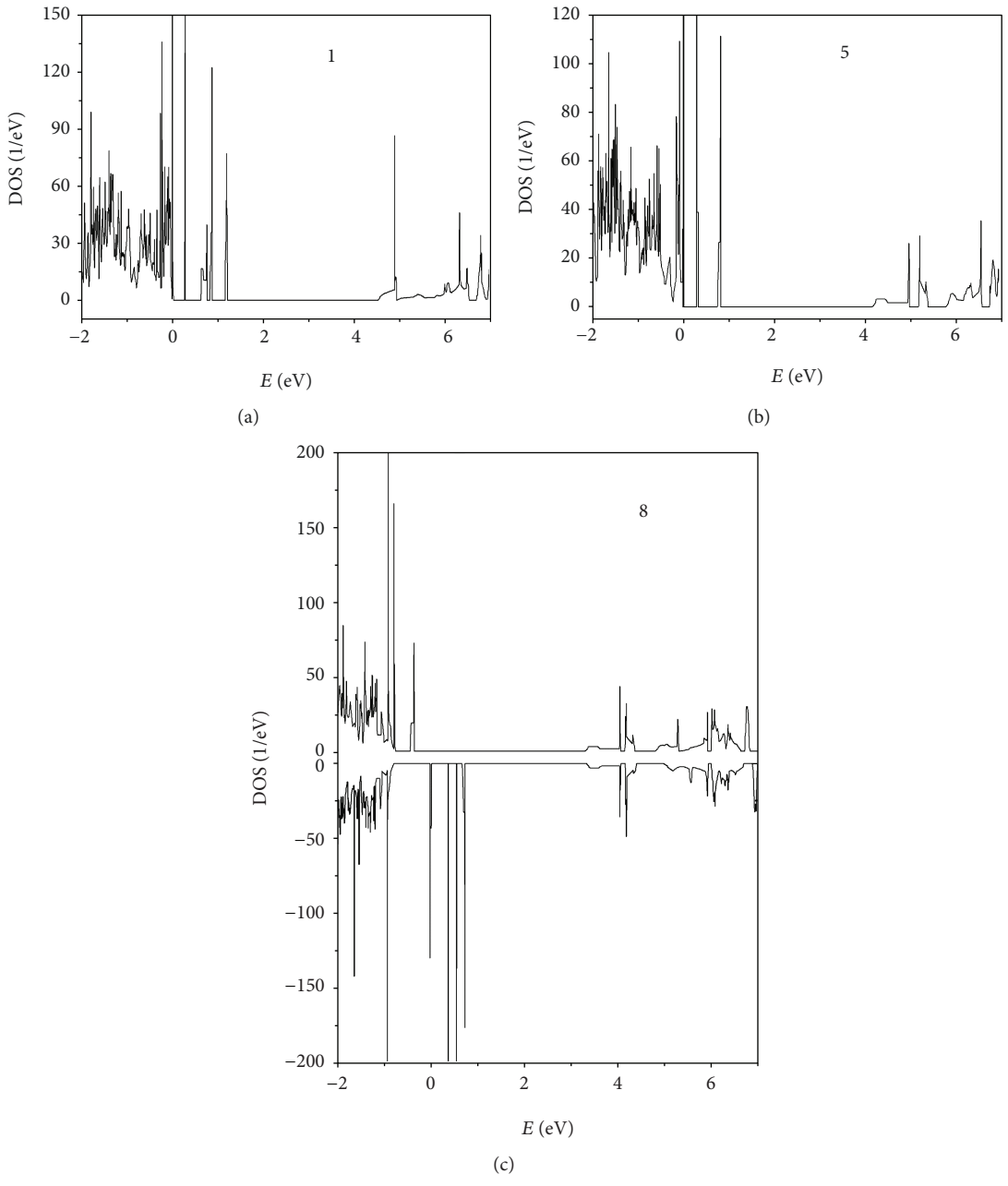

Figure 7: Total DOS plot for structures **1** (a), **5** (b), and **8** (c) identified in Figure 6.

were selected, 0 and +2. Energetically the most favourable inclusion corresponds to the (1, 0, 0) site for all the ions independently of their oxidation state. However, the highest oxidation state of the metals (Fe^{3+}, Cu^{2+}, and Zn^{2+}) was the most favoured for being incorporated into the illite structure, so those ions were selected for the rest of the discussion. The stability of those ions in the (1, 0, 0) site plays a key role in the oxygen-metal interaction, which was attested by the

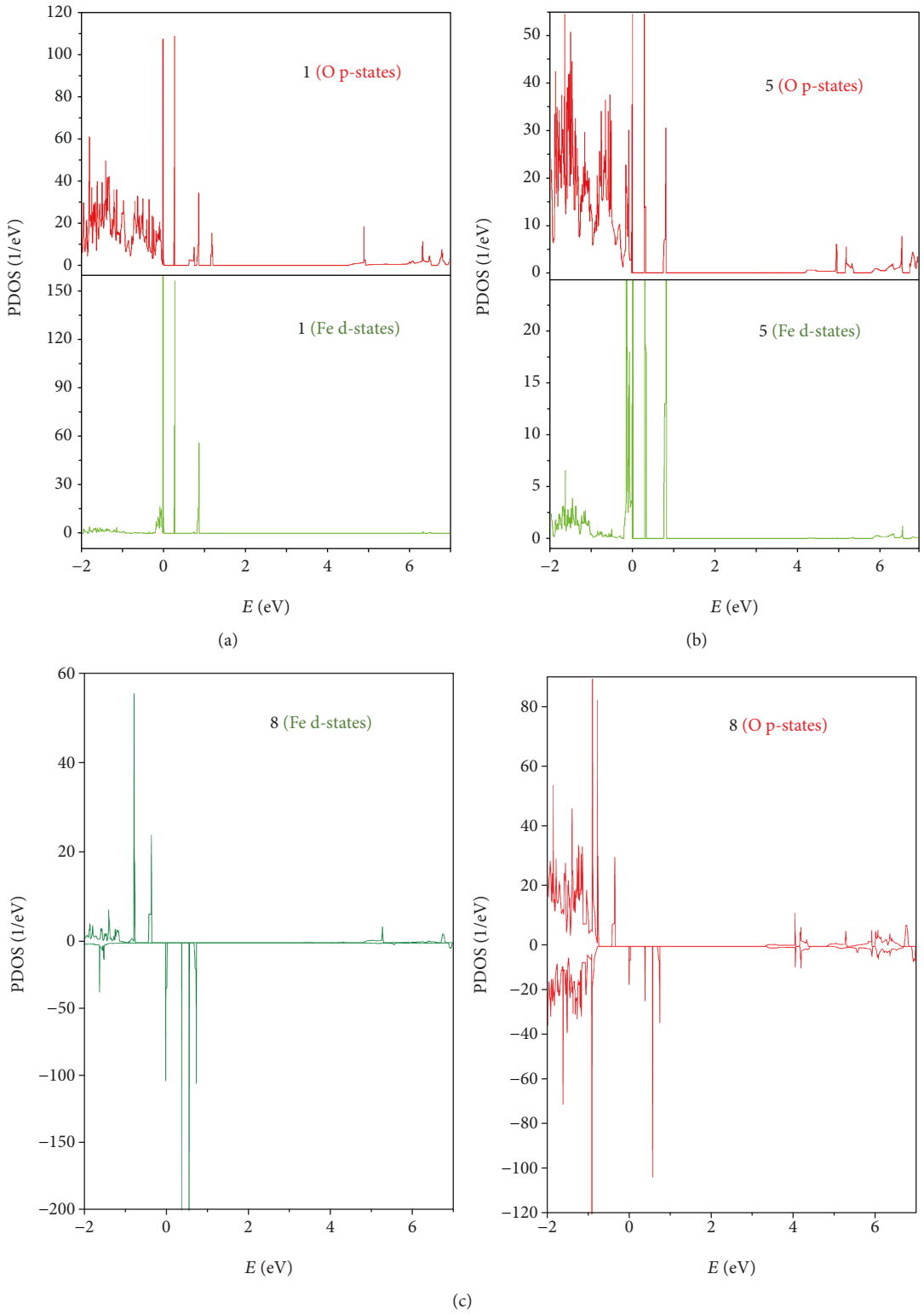

Figure 8: PDOS plot for structures **1** (a), **5** (b), and **8** (c) identified in Figure 6.

ELF and PDOS analysis. Moreover, the PDOS analysis reveals the overlapping of the oxygen p-states with the Fe and Cu d-states and Zn p-states. Thus, illite presents a good adsorption characteristic of Fe, Cu, and Zn in the (1, 0, 0) site being available for plants for its extraction by using phytoextraction or further techniques and the consequent soil regeneration. The inclusion of a second metal in the (0, 0.5, 0) site revealed the most favourable inclusion corresponding to the inclusion of the Fe^{3+} ion. The inclusion of this ion is favoured by its interaction with the two

hydroxyl groups placed around it. This interaction is corroborated by the PDOS analysis with the overlapping of the Fe d-states with O p-states. Therefore, this interaction affects the coordination sphere around the first metal as attested by the enhancement of their interatomic Al-M (M = Fe, Cu, and Zn) distance, with those metals for subsequent extraction by phytoremediation or other techniques for clean-up the soil and its regeneration being available.

Data Availability

The data used to support the findings of this study are included within the article.

Conflicts of Interest

The authors declare that there is no conflict of interest regarding the publication of this paper.

Acknowledgments

Antonio Sánchez-Coronilla thanks VPPI-US (Plan Propio de Investigación de la Universidad de Sevilla) for the financial support. Calculations were made through CICA—Centro Informático Científico de Andalucía (Spain).

References

[1] Y. Jiraskova, J. Bursik, J. Seidlerova et al., "Microstructural analysis and magnetic characterization of native and magnetically modified montmorillonite and vermiculite," *Journal of Nanomaterials*, vol. 2018, Article ID 3738106, 14 pages, 2018.

[2] D. P. Jaisi, H. Dong, and C. Liu, "Influence of biogenic Fe(II) on the extent of microbial reduction of Fe(III) in clay minerals nontronite, illite, and chlorite," *Geochimica et Cosmochimica Acta*, vol. 71, no. 5, pp. 1145–1158, 2007.

[3] J. Zhang, H. Dong, D. Liu, T. B. Fischer, S. Wang, and L. Huang, "Microbial reduction of Fe(III) in illite–smectite minerals by methanogen *Methanosarcina mazei*," *Chemical Geology*, vol. 292-293, pp. 35–44, 2012.

[4] D. Liu, P. Yuan, H. Liu et al., "High-pressure adsorption of methane on montmorillonite, kaolinite and illite," *Applied Clay Science*, vol. 85, pp. 25–30, 2013.

[5] M. Galambos, A. Krajnak, O. Rosskopfova, E. Viglasova, R. Adamcova, and P. Rajec, "Adsorption equilibrium and kinetic studies of strontium on Mg-bentonite, Fe-bentonite and illite/smectite," *Journal of Radioanalytical and Nuclear Chemistry*, vol. 298, no. 2, pp. 1031–1040, 2013.

[6] A. Romero, I. Ares, E. Ramos et al., "Mycotoxins modify the barrier function of Caco-2 cells through differential gene expression of specific claudin isoforms: protective effect of illite mineral clay," *Toxicology*, vol. 353-354, pp. 21–33, 2016.

[7] J. Chen, L. G. Yan, H. Q. Yu et al., "Efficient removal of phosphate by facile prepared magnetic diatomite and illite clay from aqueous solution," *Chemical Engineering Journal*, vol. 287, pp. 162–172, 2016.

[8] M. Akri, T. Chafik, P. Granger, P. Ayrault, and C. Batiot-Dupeyrat, "Novel nickel promoted illite clay based catalyst for autothermal dry reforming of methane," *Fuel*, vol. 178, pp. 139–147, 2016.

[9] N. Garg and J. Skibsted, "Pozzolanic reactivity of a calcined interstratified illite/smectite (70/30) clay," *Cement and Concrete Research*, vol. 79, pp. 101–111, 2016.

[10] T. T. Nguyen and P. Marschner, "Sorption of water-extractable organic carbon in various clay subsoils: effects of soil properties," *Pedosphere*, vol. 26, no. 1, pp. 55–61, 2016.

[11] A. Ksiezopolska and M. Pazur, "Surface properties of bentonite and illite complexes with humus acids," *Clay Minerals*, vol. 46, no. 1, pp. 149–156, 2011.

[12] A. S. Ramamurthy and R. Memarian, "Phytoremediation of mixed soil contaminants," *Water, Air, & Soil Pollution*, vol. 223, no. 2, pp. 511–518, 2012.

[13] K. J. Peng, C. L. Luo, Y. H. Chen, G. P. Wang, X. D. Li, and Z. G. Shen, "Cadmium and other metal uptake by *Lobelia chinensis* and *Solanum nigrum* from contaminated soils," *Bulletin of Environmental Contamination and Toxicology*, vol. 83, no. 2, pp. 260–264, 2009.

[14] H. Nacke, A. C. Gonçalves, M. A. Campagnolo et al., "Adsorption of Cu (II) and Zn (II) from water by *Jatropha curcas* L. as biosorbent," *Open Chemistry*, vol. 14, no. 1, pp. 103–117, 2016.

[15] M. J. Salazar, J. H. Rodriguez, C. V. Cid, and M. L. Pignata, "Auxin effects on Pb phytoextraction from polluted soils by *Tegetes minuta* L. and *Bidens pilosa* L.: extractive power of their root exudates," *Journal of Hazardous Materials*, vol. 311, pp. 63–69, 2016.

[16] D. Ayyappan, G. Sathiyaraj, and K. C. Ravindran, "Phytoextraction of heavy metals by *Sesuvium portulacastrum* l. a salt marsh halophyte from tannery effluent," *International Journal of Phytoremediation*, vol. 18, no. 5, pp. 453–459, 2015.

[17] M. Iqbal, A. Ahmad, M. K. A. Ansari et al., "Improving the phytoextraction capacity of plants to scavenge metal(loid)-contaminated sites," *Environmental Reviews*, vol. 23, no. 1, pp. 44–65, 2015.

[18] C. Cameselle and S. Gouveia, "Phytoremediation of mixed contaminated soil enhanced with electric current," *Journal of Hazardous Materials*, vol. 361, pp. 95–102, 2019.

[19] H. J. Shipley, K. E. Engates, and V. A. Grover, "Removal of Pb(II), Cd(II), Cu(II), and Zn(II) by hematite nanoparticles: effect of sorbent concentration, pH, temperature, and exhaustion," *Environmental Science and Pollution Research*, vol. 20, no. 3, pp. 1727–1736, 2013.

[20] V. R. Perry, E. J. Krogstad, H. El-Mayas, and S. Greipsson, "Chemically enhanced phytoextraction of lead-contaminated soils," *International Journal of Phytoremediation*, vol. 14, no. 7, pp. 703–713, 2012.

[21] E. Helios-Rybicka and R. Wojcik, "Competitive sorption/-desorption of Zn, Cd, Pb, Ni, Cu, and Cr by clay-bearing mining wastes," *Applied Clay Science*, vol. 65-66, pp. 6–13, 2012.

[22] G. Kresse and J. Furthmuller, "Efficiency of ab-initio total energy calculations for metals and semiconductors using a plane-wave basis set," *Computational Materials Science*, vol. 6, no. 1, pp. 15–50, 1996.

[23] G. Kresse and J. Furthmuller, "Efficient iterative schemes for ab initio total-energy calculations using a plane-wave basis set," *Physical Review B*, vol. 54, no. 16, pp. 11169–11186, 1996.

[24] G. Kresse and J. Hafner, "Ab initio molecular dynamics for liquid metals," *Physical Review B*, vol. 47, no. 1, pp. 558–561, 1993.

[25] G. Kresse and J. Hafner, "Ab initio molecular-dynamics simulation of the liquid-metal–amorphous-semiconductor transition

in germanium," *Physical Review B*, vol. 49, no. 20, pp. 14251–14269, 1994.

[26] V. A. Drits, B. B. Zviagina, D. K. McCarty, and A. L. Salyn, "Factors responsible for crystal-chemical variations in the solid solutions from illite to aluminoceladonite and from glauconite to celadonite," *American Mineralogist*, vol. 95, no. 2-3, pp. 348–361, 2010.

[27] K. Momma and F. Izumi, "VESTA: a three-dimensional visualization system for electronic and structural analysis," *Journal of Applied Crystallography*, vol. 41, no. 3, pp. 653–658, 2008.

[28] T. B. Terriberry, D. F. Cox, and D. A. Bowman, "A tool for the interactive 3D visualization of electronic structure in molecules and solids," *Computers & Chemistry*, vol. 26, no. 4, pp. 313–319, 2002.

[29] B. V. Kavanagh and J. P. Quirk, "The adsorption of polycationic Fe (III) species on Na-illite," *Geoderma*, vol. 21, no. 3, pp. 225–238, 1978.

[30] J. Navas, A. Sánchez-Coronilla, T. Aguilar et al., "Thermo-selective $Tm_xTi_{1-x}O_{2-x/2}$ nanoparticles: from Tm-doped anatase TiO_2 to a rutile/pyrochlore $Tm_2Ti_2O_7$ mixture. An experimental and theoretical study with a photocatalytic application," *Nanoscale*, vol. 6, no. 21, pp. 12740–12757, 2014.

[31] P. Adamo, L. Denaix, F. Terribile, and M. Zampella, "Characterization of heavy metals in contaminated volcanic soils of the Solofrana river valley (southern Italy)," *Geoderma*, vol. 117, no. 3-4, pp. 347–366, 2003.